Published in final edited form as:
Structure. 2014 June 10; 22(6): 842–853. doi:10.1016/j.str.2014.03.013.

Telomeric overhang length determines structural dynamics and accessibility to telomerase and ALT associated proteins

Helen Hwang[1,2], **Alex Kreig**[1], **Jacob Calvert**[1], **Justin Lormand**[3], **Yongho Kwon**[4], **James M. Daley**[4], **Patrick Sung**[4], **Patricia L. Opresko**[3], and **Sua Myong**[1,5,6]

[1]Bioengineering Department, University of Illinois, 1304 W. Springfield Ave. Urbana, Illinois 61801, USA

[2]Medical Scholars Program, University of Illinois, 506 South Matthews Ave. Urbana, IL 61801, USA

[3]Department of Environmental and Occupational Health, University of Pittsburgh, 100 Technology Drive Suite 326, BRIDG Pittsburgh, PA 15219, USA

[4]Department of Molecular Biophysics and Biochemistry, Yale University, 333 Cedar Street, PO Box 208024, USA

[5]Institute for Genomic Biology, University of Illinois, 1206 W. Gregory St. Urbana IL 61801, USA

[6]Physics Frontier Center (Center of Physics for Living Cells), University of Illinois, 1110 W. Green St. Urbana IL 61801, USA

Abstract

The G-rich single stranded DNA at the 3′ end of human telomeres can self-fold into G-quaduplex (GQ). However, telomere lengthening by telomerase or the recombination-based alternative lengthening of telomere (ALT) mechanism requires protein loading on the overhang. Using single molecule fluorescence spectroscopy we discovered that lengthening the telomeric overhang also increased the rate of dynamic exchanges between structural conformations. Overhangs with five to seven TTAGGG repeats, compared to four repeats, showed much greater dynamics and accessibility to telomerase binding and activity, and loading of the ALT-associated proteins RAD51, WRN and BLM. Although the eight repeats are highly dynamic, they can fold into two GQs, which limited protein accessibility. In contrast, the telomere-specific protein, POT1 is unique in that it binds independently of repeat number. Our results suggest that the telomeric overhang length and dynamics may contribute to the regulation of telomere extension via telomerase action and the ALT mechanism.

*Correspondence should be addressed to S.M. (smyong@illinois.edu) .

INTRODUCTION

Human telomeres terminate in a 50-200 nucleotide single-stranded 3′ overhang that plays a pivotal role in chromosome end protection (Makarov et al., 1997; McElligott and Wellinger, 1997; Wright et al., 1997). The G-rich overhang serves as the substrate for telomerase which extends telomeres by adding tandem TTAGGG repeats(Greider and Blackburn, 1987) and as a binding site for the POT1 protein which prevents the activation of the checkpoint kinase ATR, inhibits sister chromatid fusion, and represses homologous recombination (Denchi and de Lange, 2007; Hockemeyer et al., 2006; Palm et al., 2009; Wu et al., 2006). Furthermore, the telomeric overhang invades the duplex region forming a t-loop(Griffith et al., 1999) and thereby blocking ATR and ATM signaling which is essential to prevent the chromosome end from being incorrectly recognized as a DNA double strand break (de Lange, 2009).

Owing to the end-replication problem, the ends of chromosome shorten with each round of DNA replication in all somatic cells (Harley et al., 1990; Watson, 1972). The progressive telomere attrition results in replicative senescence, growth arrest or apoptosis (Karlseder et al., 1999; Smogorzewska and de Lange, 2002). Cancer cells, however, overcome this barrier mostly (85-90%) by upregulating telomerase activity to sustain the telomere length (Kim et al., 1994; Shay and Bacchetti, 1997). Nevertheless, significant subset (10-15%) of cancers that are telomerase-negative lengthen telomeres by a telomerase-independent mechanism, termed Alternative Lengthening of Telomeres (ALT) (Bryan et al., 1997; Bryan et al., 1995; Cesare and Reddel, 2010). ALT is likely mediated by homologous recombination (HR) mechanisms (Dunham et al., 2000; Lundblad and Blackburn, 1993; Varley et al., 2002). Numerous proteins involved in telomere function, HR, DNA damage repair and DNA replication are associated with ALT (Cesare and Reddel, 2008). Therefore, all cancer cells exhibit indefinite lifespan supported by either the telomerase-catalyzed extension or ALT-mediated lengthening of telomeres. Due to this common feature of all cancers, telomeres and telomere-associated proteins have been attractive drug targets for anti-cancer therapy (Shay and Bacchetti, 1997; Shay and Wright, 2002; Tarkanyi and Aradi, 2008).

The telomeric overhang presents a highly vulnerable target which can be misrecognized to induce a DNA damage response that can lead to chromosome fusion and erosion (d'Adda di Fagagna et al., 2004; Harley et al., 1990; Lingner et al., 1995; Palm and de Lange, 2008; Shampay et al., 1984). Therefore, the capping and protection of the telomeric overhang is of utmost importance for genome integrity. From Schizosaccharomyces pombe to humans, the overhang is specifically bound by the shelterin component POT1, which prevents ssDNA stimulated repair and recombination (Denchi and de Lange, 2007; Hockemeyer et al., 2005). Furthermore, POT1 regulates access to the overhang to facilitate complete chromosome replication (Colgin et al., 2003; Lei et al., 2005; Shakirov et al., 2005; Ye et al., 2004).

While many proteins need to gain access to the telomere overhang for maintenance and lengthening, the G-quadruplex structure that can form in successive repeats of TTAGGG may serve as a structural barrier to protein access. Recent reports provide strong evidence that G-quadruplexes form in cells including at telomeres (Biffi et al., 2013; Paeschke et al., 2013; Paeschke et al., 2011; Sfeir et al., 2009; Vannier et al., 2012). Structural studies show that in the presence of K+ or Na+ ions, four TTAGGG repeats fold into stable G-

quadruplexes consisting of three tetrads of four guanines interacting via Hoogsteen base pairing (Hardin et al., 1991; Hardin et al., 1992). Oligonucleotides with four TTAGGG repeats are poor substrates for telomerase due to G-quadruplex folding (Wang et al., 2011). However, the current view of telomeric overhang structure is incomplete because it derives largely from images of static molecules with four or fewer telomeric repeats.

Using highly sensitive single molecule techniques, we have examined the folding behavior of overhangs with varying numbers of telomeric repeats (4-8) and how this behavior relates to overhang accessibility to proteins involved in telomere processing. We observed that the overhang structural dynamics increased as a function of length, and that the dynamic properties influenced overhang accessibility. We investigated loading of several ALT-associated proteins, along with POT1 and telomerase, both of which bind telomere overhangs in a sequence specific manner. Our results reveal that overhangs with four TTAGGG repeats fold into a stable G-quadruplex and are poor substrates for protein loading. In contrast, five to seven repeat overhangs exhibit significantly higher dynamics and corresponding accessibility to most of the molecules tested. Collectively, our observations point to the importance of the dynamics of G-quadruplex structures located at 3′ overhangs in governing the processing of telomeres by proteins involved in telomere lengthening mechanisms.

RESULTS

Telomere overhangs longer than four repeats display multiple conformations and dynamics

Although numerous studies have examined the folding kinetics of human G-quadruplex (GQ), studies of physiologically relevant telomeric substrates that have more than four repeats of TTAGGG are limited (Bauer et al., 2011; Lane et al., 2008; Vorlickova et al., 2005). Melting temperature and circular dichroism experiments have suggested that GQs are blocks that resemble “beads-on-a string” and that they can move independently of each other and are constrained only by connecting linkers (Petraccone et al., 2011; Yu et al., 2006). In addition, molecules with telomeric repeats in multiples of four exhibit increased enthalpy and entropy arising from stable GQ formation (Yu et al., 2006). On the contrary, a previous AFM study showed that long telomeric 3′ overhangs did not form the maximum number of GQs. Rather, they were dispersed, suggesting that GQ folding of overhangs longer than 4 repeats may be dynamic (Wang et al., 2010).

To investigate the effect of telomere repeat length on GQ conformation, we prepared a series of 3′ overhang DNA substrates with varying numbers of TTAGGG repeats from 4 to 8, which we refer to as G4-G8 hereafter. Each DNA was labeled with two fluorescent dyes, Cy3 and Cy5 at both ends of the ssDNA for measuring FRET (Fluorescence Resonance Energy Transfer). FRET, as a molecular ruler, reports on the folding status of the telomeric overhang such that a high FRET signal indicates GQ folding in G4 DNA (Figure 1A). In 100 mM KCl, we obtained one, two, and four FRET peaks for molecules with four (G4), five (G5), and six (G6) telomeric repeats respectively (Figure 1B). Each FRET histogram was built from FRET values of over 5000 individual molecules. We interpret the discrete FRET peaks as reflecting formation of one, two and four conformations in G4, G5 and G6,

respectively. It is plausible that G5, for example folds up in two different ways i.e GQ consisting of repeats 1-4 or 2-5, yielding two distinct FRET states. With seven telomeric repeats (G7), we observed a broad FRET histogram, likely due to formation of multiple conformations arising from various ways of GQ folding that yield a wide range of dye to dye distance. For G8, we also obtained a broad FRET distribution, yet with a prominent high FRET peak. Based on the total length of single stranded DNA of 48 nucleotide in G8, this high FRET far exceeds the expected FRET value (below 0.2) in this buffer condition (Murphy et al., 2004). Therefore, the unusually high FRET in G8 is likely due to the formation of two GQs from two sets of four repeats (Figure 1B).

To confirm that the high FRET state represents folded GQ DNA, we examined overhang dynamics in various monovalent salts. K+ and Na+ stabilize GQ folds by coordinating in the central channel of the tetrads, however, the smaller Li+ ions do not support GQ folding (He et al., 2005; Wong and Wu, 2003). As expected, 100mM NaCl induced similar distributions of GQ conformations for G4-G8 as we obtained for 100mM KCl conditions (Figure S1). We note that the slight differences obtained for NaCl and KCl is likely due to different conformations of GQ in sodium and potassium ion as reported previously (Ambrus et al., 2006). In contrast to KCl and NaCl, 100mM LiCl induced broad FRET peaks for all overhang lengths with overall lower FRET values, reflecting no discrete folding of GQs. To test the sequence dependent folding of GQ, we prepared G4 and G8 mutants which bear “TTAGCG (instead of TTAGGG) at the 4^{th} and 8^{th} repeat, respectively. Both mutants, which differ from G4 and G8 by only a single nucleotide, resulted in a completely different FRET distribution that reflect lower FRET unfolded states, similar to the LiCl condition. This confirms that the high FRET peak for the G8 overhang in KCl and NaCl likely represents two folded GQs, since mutating the last repeat eliminates the high FRET peak even though a GQ could still form between repeats 1 to 7.

Next, we sought to probe the real-time dynamics in G4-G8 DNA by analyzing the single molecule traces. The representative single molecule trace for G4 shows that it stays in one high FRET state, which is consistent with the histogram. The G5 and G6 overhangs, however displays two and four FRET states in exchange, respectively, likely representing different conformations arising from alternative folding of GQ. G7 and G8 traces exhibit many more FRET states, reflecting dynamic exchanges amongst multiple conformations (Figure 1C). In addition, the rate at which conformations exchange becomes faster for longer overhangs. To quantify this effect, we collected dwell times (δt, Figure 1C) from about 200 molecules for each DNA and fitted the data to an exponential decay. The halftlife, $t_{1/2}$ obtained from the fit reveals that the fastest dynamic in G8 is one order of magnitude higher than the slowest time obtained for G5. These faster dynamics observed for the longer overhangs indicates that increased repeat number induces more rapid exchanges (Figure 1D, Figure S1). Taken together, telomeric overhangs longer than four repeats exhibit dynamic folding states and the longer lengths induce more complex conformations and faster dynamics. Interestingly, despite the fast conformational dynamics, overhangs with eight repeats display frequent transitions to the high FRET state, likely arising from the formation of two GQs.

GQ dynamics modulate overhang accessibility to complementary DNA

A short antisense strand of the telomeric sequence is frequently used to test unfolding of GQ structures by forming duplex DNA with the unfolded molecules (Wang et al., 2010; Zaug et al., 2005). In addition, antisense telomeric DNA exists in ALT cells in the form of c-circles and has been employed as a specific and quantifiable marker of ALT activity in vivo (Henson et al., 2009). We applied a similar 12 nt C2 complementary antisense $(CCCTAA)_2$, molecule in excess (10nM) to test the accessibility of the G4-G8 overhangs. We note that the annealing experiment was performed at room temperature without adding any external source of heat. The FRET values from over one thousand molecules were taken before and 10 minutes after the addition of C2 DNA.Binding of C2 is expected to result in a FRET decrease (Figure 2A). The FRET histograms were prepared from data collected before and after C2 incubation, shown in dark gray and light blue, respectively (Figure 2B). As a positive control, we included G3TTAG, a G4 overhang devoid of the two terminal Gs that cannot fold into GQ (Hwang et al., 2012). The histogram for G3TTAG, G6 and G7 showed a substantial shift to lower FRET values while G4, G5 and G8 remained nearly unchanged after C2 incubation (Figure 2B). The lower FRET states upon C2 binding for the G6 and G7 overhangs are also broadly distributed, reflecting multiple conformations as seen before. The percent accessibility was calculated by subtracting the histogram before C2 addition from the histogram after the addition of C2, indicating the percentage of molecules that have C2 bound (Figure S2A, B). The same experiment was performed at an ensemble level using a fluorometer, from which the accessibility was calculated by the % change in FRET value before and after C2 addition. The same pattern of accessibility emerged from the two sets of data, both pointing to a limited accessibility in G4, G5 and G8 molecules and increased accessibility for G6 and G7. G5 was slightly more accessible than G4, which is consistent with increased folding dynamics compared to G4. As evident from the data, G3TTAG represents the most accessible substrate due to the lack of GQ folding. Despite high dynamics in folding, G8 was largely inaccessible, likely due to the ability to form two GQs.

To determine whether stable GQ folding was responsible for the limited C2 binding to G4, G5 and G8, we repeated the experiments in the presence of 100mM NaCl and 100 mM LiCl. As expected, the similar pattern of accessibility was also obtained in the 100mM NaCl condition where GQ structures resemble that of KCl condition (Figure S2B). In LiCl where the GQ folding is unstable, the C2 accessibility to G4, G5 and G8 was as high as for the control G3TTAG substrate (Figure S2C). Furthermore, the G4 and G8 mutants with a single nucleotide change to prevent one or two stable GQ folds, respectively, also displayed high accessibility to C2 (Figure S2D). In both the LiCl and mutant cases, the lack of stable GQ folding is likely responsible for the increased accessibility to C2 strand binding for all substrates.

To gain structural insight into C2 binding, we examined GQ images captured by atomic force microscopy (AFM). We compared the least accessible substrate, G4, to one of the most accessible substrates, G6. The G4 and G6 molecules pre-incubated with C2 appear as a sharp peak representing the folded GQ (Figure 2D). We note that the two peaks in Figure 2D represent two individual G4 molecules, both of which yield a single sharp peak and the same is true for G6 peaks. Unlike a single peak arising from G4, the G6 peak possesses a shoulder

peak that likely represents C2 binding (Figure 2E). We confirmed that the shoulder peak only occurs in G6 incubated with C2, but not in G4. This is shown in the histograms where the width of G4, G4+C2, G6 and G6+C2 are collected from about one hundred molecules and plotted as a molecular frequency (Figure 2F). This data provides structural evidence that while G6 is accessible to C2 binding, the G4 molecule is not.

GQ conformation influences RAD51 access

RAD51 is a key player in the homology-directed repair that triggers ALT pathway (Oganesian and Karlseder, 2011). Furthermore, the inhibition of RAD51 synthesis leads to telomere erosion and chromosome fusion, suggesting an important role of RAD51 in telomere maintenance (Tarsounas et al., 2004). We sought to examine if GQ folding and dynamics modulate RAD51's ability to bind and resolve the GQ conformation (Figure 3A, top). RAD51 addition to all substrates induced a substantial shift in FRET, except for the G4 substrate. The emergence of low FRET states upon RAD51 addition in all cases is likely due to the filament formation expected from RAD51 binding (Figure 3B). G4 showed the lowest accessibility, suggesting the presence of a stable GQ fold which limits RAD51 binding. The percent accessibility resulting from all overhang lengths shows an overall resemblance to C2 anti-sense accessibility with the largest difference observed in G8 (Figure 3C, orange bars). Unlike the case of C2 binding, G8 yields high accessibility to RAD51, likely due to the small DNA binding size of RAD51. RAD51 is a structural homolog of the E. coli RecA recombinase that engages 3 nt (Chen et al., 2008; Shin et al., 2003) of DNA per protein monomer to form a filament (Arata et al., 2009; Hilario et al., 2009; van Mameren et al., 2009). Therefore, the higher accessibility shown for RAD51 than C2 may be explained at least in part by the different lengths of single stranded DNA required for RAD51 (3 nt) compared to C2 (12 nt) binding.

WRN and BLM access to telomeric overhangs depend on the GQ folding dynamics

Human RecQ-family helicases Werner (WRN) and Bloom (BLM) can unwind GQs in vitro, with high specificity (Liu et al., 2010; Mohaghegh et al., 2001). BLM, in conjunction with RAD51 can interact with TRF2 in ALT-activated cells to promote telomere elongation (Stavropoulos et al., 2002), while WRN is directly involved with telomeric recombination in the ALT pathway (Mendez-Bermudez et al., 2012). However, both WRN and BLM require a 3′ ssDNA tail to unwind a G-quadruplex (Mohaghegh et al., 2001). To determine whether overhang length influences WRN and BLM loading and activity, we applied both proteins to the overhang substrates (G4 to G8) and monitored potential FRET decreases as indicative of protein loading and GQ unwinding (Figure 3A, bottom). The FRET histograms collected after addition of WRN and ATP displayed a negligible (< 10%) shift for G4 and G8 while a significant change was observed for G5, G6 and G7 (Figure S3A). The same pattern was also seen for BLM (Figure S3B). To further examine the ATP dependence of the protein loading, we applied WRN to the same set of DNA constructs in the absence of ATP and in the presence of the non-hyrolyzable analog ATPγS. The accessibility data indicates that WRN does not bind in the absence of ATP, but the binding occurs to a similar degree in the ATP condition compared to the presence of ATPγS albeit reduced (Figure S3C). Taken together, we demonstrate that the GQ folding in G4 and G8 are the least accessible to RecQ

helicase loading, whereas G5 to G7 yield substantially higher accessibility, similar to C2 anti-sense binding (Figure 3C).

POT1 binding is independent of GQ folding and overhang length

Protection of Telomeres-1 (POT1) is a member of shelterin complex that guards and controls the single stranded telomeric overhang (Denchi and de Lange, 2007). POT1 engages with the telomeric overhang in a sequence specific manner (TTAGGGTTAG) as clearly demonstrated by the high resolution structure and biochemical characterization (Lei et al., 2004). Recently, we reported that POT1 binds and thereby unfolds GQ in a stepwise fashion in which one monomer binds TTAGGGTTAG in two successive steps (Hwang et al., 2012). In the previous study, we used shorter overhang lengths, G2 to G4, to focus on the detailed monomer binding steps. In the current study, we use G4 to G8 to test if POT1 binding is influenced by GQ folding and dynamics exhibited in the longer overhang (Figure 4A). The FRET histogram obtained after adding POT1 clearly shows that POT1 binding occurred to a similar degree for all overhang lengths (Figures 4B, C). POT1 displayed a binding mode that was independent of the inherent conformational states and dynamics governed by the repeat number, in contrast to the repeat number dependent loading exhibited by C2, RAD51, WRN and BLM.

Telomerase loading and extension activity is modulated by GQ dynamics

GQ structures inhibit telomerase activity (Salazar et al., 1996; Zahler et al., 1991), hence the anti-cancer therapy efforts in developing drugs that stabilize GQ. The sequence specific binding of telomerase to the telomere is achieved by the complementarity between the telomeric overhang and the RNA template embedded in the catalytic site of telomerase (Weinrich et al., 1997). In this respect, telomerase shares similarity with POT1. To examine telomerase activity, we used an established telomerase isolation protocol. HEK 293T cells were transfected with flag-tagged telomerase overexpression plasmids (generous gift from Tom Cech) (Latrick and Cech, 2010). The cell lysate was applied to a single molecule surface pretreated with anti-flag antibody (α-flag) to pull down the flag-tagged telomerase (Jain et al., 2011). The pull-down efficiency was tested by applying the primary antibody against telomerase followed by red (Alexa 647) labeled secondary antibody (Figure 5A). The red fluorescent spots appeared only when all the components were present and were not detected above background when any of α-flag, cell lysate or primary antibody was omitted, indicating the highly specific capture of telomerase (Figures 5B, C).

We used this platform to evaluate overhang accessibility by applying green (Cy3) labeled DNA followed by the primary and red labeled secondary antibody used above (Figure 5D). By co-localizing the green and red signals, we were able to count the number of telomerase molecules occupied by the corresponding DNA. The fraction of red molecules that co-localize with green was used to calculate the percent occupancy of telomerase bound to DNA (Figure 5E). The resulting bar graph reveals that G4 and G8 are less occupied by telomerase than G3TTAG, G6 and G7, indicating a similar pattern of accessibility seen for C2 and the helicases. The limited occupancy by G4 and G8 coupled with the enhanced binding by G6 and G7 points to a loading mechanism of telomerase that relies on the conformational dynamics of the telomeric overhang.

Next, we asked if the telomerase extension activity reflected the overhang length dependency of telomerase binding. We performed a modified version of primer extension assay in which flag-telomerase was immunoprecipitated onto α-flag coated beads and the telomere extension was stimulated by adding the individual DNA template and mix of dNTPs including radiolabeled dGTP. The reaction was carried out in the same buffer condition used for the single molecule assay at 37°C for one hour until the reaction was quenched and analyzed by 12% PAGE (Figure 5F). We quantified the product of telomerase extension by Image J and ImageQuant software. The total intensity collected for each DNA was normalized by the total intensity obtained for G3TTAG, a positive control DNA template that leads to the highest extension activity (Berman et al., 2011; Latrick and Cech, 2010). As shown, the telomerase extension also exhibits the similar length dependency with limited activity for G4 and G8 and a significantly higher activity measured for G5-G7 (Figure 5G), suggesting that the telomerase loading to telomeric overhang may contribute to the level of telomerase extension. The slight differences observed between the accessibility of DNA and the telomerase activity can be due to several factors. It is possible that not all the substrates bound to telomerase in the single molecule surface are productive i.e engaged in correct orientation or position sufficient to yield telomerase activity. Further, the ability of G8 to fold into two GQ structures may impact the ability of telomerase to engage the overhang in the enzyme active site for telomere extension.

DISCUSSION

Early work suggested that the formation of GQ at the telomeric overhang limits access of telomerase and other telomere binding proteins (Burger et al., 2005; Gomez et al., 2006a; Gomez et al., 2006b; Phatak et al., 2007; Tahara et al., 2006). Furthermore, DMS footprinting study demonstrated that the GQ preferentially forms at the end of a 3′ overhang rather than at the internal positions, suggesting that the GQ formation at the end position may inhibit telomerase and ALT mediated telomere lengthening (Tang et al., 2008). Using single molecule approaches we discovered that the telomere overhang length greatly influences the dynamics of GQ unfolding. We sought to examine how DNA conformational dynamics influences the accessibility of telomeric overhangs to proteins that are relevant for telomere protection and lengthening. We observed that in general, increasing overhang length led to increased conformational dynamics and greater accessibility to protein loading. However, we also note interesting exceptions. First, the overhangs consisting of multiples of four repeats were the least accessible regardless of length. We further confirmed this effect by control measurements. In ionic conditions that stabilize GQ (NaCl and KCl), the G4 and G8 remain inaccessible whereas they become fully accessible to complementary DNA (C2) binding in LiCl buffer which destabilizes GQ. Further, the GQ folding is disrupted by a single nucleotide mutation in both G4 and G8 cases, making them fully accessible to C2 binding. Second, the binding of the telomeric protein POT1 was not influenced by overhang length or dynamics. In light of the intimate contact between POT1 and telomeric overhang DNA displayed in their structure (Lei et al., 2004), it is not surprising to observe that POT1 can actively disrupt the GQ folding. Collectively, these studies indicate that telomere overhang length modulates telomere processing with the exception of POT1.

The single molecule FRET employed here is an ideal approach in several respects. First, the range of distance change induced by GQ folding and unfolding is within the FRET sensitive detection range. Second, single molecule detection enables the resolution of various conformers of GQ exhibited by the different overhang lengths. Although we cannot identify the exact conformations represented by different FRET values, the overall histogram obtained for G4, G5, G6, G7 and G8 reveals one, two, four and multiple states, respectively, as can be expected from alternate pairings of G-triplets (Figure 1B). Although different FRET values observed in G5-G7 do not inform us about the exact conformations, we predict that the GQ formed by neighboring G-triplets contributes to the various folding states. For example, there are three ways that G6 can fold by pairing up of repeats 1-4, 2-5, 3-6 and the fourth state can result from a flanking of the single stranded portion of DNA. Third, single molecule traces reveal the real-time molecular dynamics of GQ as it undergoes conformational changes by itself (Figure 1C). Individual single molecule traces of G5-8 reveal that they are in dynamic exchange with alternate conformers and that the rate of exchange is accelerated as the repeat number increases (Figures. 1C, D). While the conformers appear to be evenly distributed amongst different conformers in G5-G7, G8 displays a pronounced high FRET peak which exceeds the other states (Figure 1B). We interpret this high FRET as arising from two GQs forming on G8, which in turn yields low accessibility to several proteins tested herein. Consistent with this, mutation of the 8th repeat prevent two GQs from folding and eliminates this high FRET peak, even though a single GQ fold can still form among repeats 1 through 7. It is interesting to note that G8 exhibits both the high propensity for folding and the fast dynamic behavior. While small proteins such as RAD51 gains access to such construct, most other proteins had a significantly reduced access to G8.

The conformational dynamics of DNA and its length dependent accessibility to various proteins may have implications for when the telomeric overhang becomes exposed during replication, for example. Although it may be transient, the free single strand overhang is expected to exhibit conformational dynamics while proteins such as POT1, telomerase and ALT associated proteins will compete for binding to the same overhang. Based on our result, the number of TTAGGG repeats at the very end of an individual telomere will influence its conformational dynamics and the corresponding level of accessibility to the available proteins. Depending on which protein gains access, the telomere will face different outcomes. If the end is bound by telomerase, it will be extended whereas if the end is accessed by RAD51, the end may undergo a homology directed repair pathway (Cesare and Reddel, 2008; Henson et al., 2002). However, in normal somatic cells, it is likely that the telomeric end is readily occupied by POT1. In a cell, the folding of a telomeric overhang into a GQ converts it to substrate for binding by various proteins that can interact with GQ structures and compete for loading. However, evidence shows that POT1 can effectively compete for loading on the telomeric overhang due to telomere tethering by shelterin TPP1-TIN2 (Takai et al., 2011). TPP1 also recruits telomerase to the telomeres in a cell cycle regulated matter (Zhang et al., 2013). Therefore, the status of the shelterin complex at the telomere contributes to protein recruitment and loading on the overhang. Our data indicate that overhang structural dynamics also contribute to regulating protein accessibility.

Importantly, we showed that POT1 can load on telomeric overhangs that are pre-folded in a GQ, including the G4 and G8 substrates (Figure 4).

Taken together, we have provided in vitro evidence that GQ folding at the 3′ end of the telomeric overhang plays a critical role in controlling protein access. All ALT associated proteins tested here show the length-dependent loading that resembles C2 binding with the exception of RAD51 which readily gains access to G8 which renders low accessibility to all other proteins tested. In contrast, POT1 bound the G4-G8 substrates with equal efficiency, clearly indicating a different binding mode that leads to active disruption of GQ (Hwang et al., 2012; Wang et al., 2010; Zaug et al., 2005). A better understanding of the mechanisms for regulating chromosome end structure and accessibility will help identify new targets for anti-cancer therapies, with improved specificity for telomeres. Furthermore, our single molecule platform provides a screening tool for testing the current and future generation GQ ligands, thereby assessing anticancer drugs with single molecular sensitivity. Many factors likely contribute to the regulation of telomere lengthening by ALT or telomerase, and our data provide evidence that telomere overhang length is one factor that may contribute to this regulation.

MATERIALS AND METHODS

Ensemble C2 Measurements

Bulk measurements were performed at room temperature 24 ± 1°C in a standard, G-quadruplex formation reaction condition: 100mM KCl, 100mM Tris, with a 10nM partial duplexed telomeric DNA sample. The reaction was initiated with 1nM of C2 DNA. FRET efficiency, E, was monitored with a fluorescence spectrophotometer (Cary Eclipse, Varian). Accessibility of G-quadruplex DNA was determined by comparing DNA-only FRET efficiency, E_{DNA}, with steady-state efficiency after C2 addition, E_{C2+DNA} according to:

$$\frac{E_{DNA} - E_{C2+DNA}}{E_{DNA}}.$$

AFM Sample Preparation and Imaging

DNA substrates were diluted to 2ng/uL in reaction buffer with additional 10 mM MgCl2. All samples were incubated at room temperature for 15 minutes. Samples were deposited on freshly cleaved mica (Ted Pella, Redding, California), followed by a wash with deionized water and drying with nitrogen. Imaging was performed on a Cypher AFM (Asylum Research, Santa Barbara, CA) in tapping mode. AC160TS AC mode silicon probes with spring constants of ~42 newtons/m and resonance frequencies of 300 kHz were used. Images were captured at a scan size of 1 um by 1 um with a resolution of 1024 by 1024 pixels.

Protein Purification and Reaction Conditions

RAD51 was purified in a similar way described previously(Sigurdsson et al., 2001). Single molecule experiments were done at 37C and used 1uM RAD51 with reaction buffer containing 50mM KCl, 1mM MgCl2, and 1mM ATP. The purified hetrotrimer RPA was a kindly provided by Dr. Walter Chazin (Vanderbilt University)(Arunkumar et al., 2005). The reaction used 1uM RPA with 100mM KCl and 10 mM Tris. WRN proteins were purified as

described previously (Opresko et al., 2009). Reactions were performed in 25mM KCl, 1mM MgCl2, 10mM Tris pH 7.5, and 2mM ATP. BLM was purified as described previously(Bussen et al., 2007) and single molecule reactions were performed with 100nM BLM in the presence of 3mM MgCl2 20mM Tris pH 7.6, 50mM KCl, and 2mM ATP.

Gel Mobility Shift assay

10nM partial duplex telomeric overhang was mixed with and without 200nM RPA with Cy5 dyes at the junction and incubated for 15 minutes at 37C with 2mM MgCl2, 10mM Tris pH 7.6, and 50mM KCl. The reaction mixture was loaded and ran on a 6% acrylamide gel 65V for 2 hours with 0.5× TBE running buffer. Analysis in Image J was used to quantitate accessibility percentages by taking the area of DNA with RPA and normalizing it to the areas of the sum of DNA with RPA and DNA alone.

Telomerase overexpression

Over-expression of telomerase was carried out using modification to an established protocol (Cristofari and Lingner, 2006). Cell lysate containing recombinant telomerase was reconstituted in HEK293T cells by over-expressing hTR and 3xFLAG tagged hTERT genes in pBS-U1-hTR and pVan107 respectively (generous gifts from Dr. Thomas Cech). Cells were grown to 90% confluency containing DMEM medium (Gibco) supplemented with 10% FBS (Gibco) and 1% Pen Strep (Gibco) at 37°C and 5% CO2. Cells were transfected with 10μg of pBS-U1-hTR plasmid and 2.5 μg pVan107 plasmid diluted in 625 μl Opti-MEM (Gibco) using 25 μl Lipofectamine 2000 (Invitrogen) diluted in 625 μl Opti-MEM according to the manufacturer's instruction. Cells were allowed to grow for 48 hours post-transfection, at which point they were trypsinized and washed with phosphate buffered saline and lysed using 500 μl Chaps lysis buffer (10mM Tris-HCl, 1mM MgCl2, 1mM EDTA, 0.5% CHAPS, 10% Glycerol, 5mM β-Mercaptoethanol, 120U Promega RNasin plus, 1μg/ml pepstatin, aprotinin, leupeptin, chymostatin, and 1mM AEBSF). Cell lysate was then either flash frozen in liquid nitrogen and stored at −80°C, or immunopurified.

Immunopurification of telomerase

Telomerase enzyme was immunopurified from cell lysate using anti-flag M2 affinity gel (Sigma). Prior to addition of the affinity gel to the cell lysate, 40μl of affinity gel beads were washed three times with 40μl of 1× human telomerase buffer (50mM Tris-HCl pH8, 50mM KCl, 1mM MgCl2, 1mM spermidine, 5mM β-Mercaptoethanol, and 30% glycerol) by centrifugation at 4000 RPM for 1 minute at RT followed by removal of the 40μl supernatant. Following washes, 80μl of affinity gel-human telomerase buffer slurry was added to the 500μl cell lysate and placed on a rotator for 3 hours at 4°C. After centrifugation at 4000 RPM and removal of liquid the beads were washed three times with 1× human telomerase buffer, and flash frozen in liquid nitrogen as 80μl of bead slurry in 1× human telomerase buffer and stored at −80°C.

Single Molecule Pull-down of Telomerase and Co-localization with Telomeric DNA

We utilized single molecule pull-down methods to pull down the telomerase complex from over expressed telomerase cell lysate(Jain et al., 2011).

Telomerase was isolated on the biotinated-PEG coated quartz surface in the following order: Streptavidin, 1:50 antiflag antibody (Sigma, mouse M2, F9291), 1:200 cell lysate, 1:100 primary hTERT antibody (Abcam, rabbit monoclonal), and 1:10,000 secondary antibody labeled with Alexa647 (Jackson Immunoresearch, donkey anti-rabbit).

Each step was incubated for 15-30 minutes and 200uL of telomerase reaction buffer (50mM Tris-Cl pH8, 50mM KCl, 1mM MgCl2) was flowed in to wash out unbound molecules in between each addition. The channels without anti-flag antibodies, primary antibodies, or cell lysate showed <50 fluorescent spots per imaging area of 2500um^2, possibly due to surface impurities.

To check the binding affinity of telomerase to DNA, 1nM of the partial duplex telomeric DNA labeled with Cy3 was incubated with the isolated telomerase on the surface prior to the addition of antibodies. It was then washed before the hTERT primary and Alexa647 secondary antibodies were added.

Telomerase extension assay

The telomerase extension assay was a modification of a previously described protocol (Zaug et al., 2010).The telomerase extension reaction mixture (20μl) contained 1× human telomerase buffer (described above), 2μl of 3000 Ci/mMole 32P-dGTP (Perkin Elmer), 0.058mM dGTP, 10mM dTTP, 10mM dATP, 1uM telomeric partial duplex DNA substrate and 6μl immunopurified telomerase complex. Reactions were incubated for 1 hour at 30°C, then stopped with the addition of 2μl 0.5M EDTA and heat inactivated at 65°C for 20 minutes. 8.0 fmol of a 37-mer loading control was added prior to purification of the sample using an Illustra microspin G-25 column (GE Life sciences) followed by the addition of 15μl of loading buffer (94% formamide, 0.1× TBE, 0.1% bromophenol blue, 0.1% xylene cyanol) to 15μl of sample. The heat denatured (10minutes, 100°C) samples were loaded onto a 10 % denaturing acrylamide gel (8M urea, 1xTBE) for electrophoresis. 32P incorporation was imaged using a phosphor screen and phosphorimager (GE Healthcare). Total activity was quantitated using ImageJ and ImageQuant and normalized to a loading control as established previously(Jain et al., 2011; Latrick and Cech, 2010). Briefly, each band is individually quantitated, summed, and normalized to the activity seen with the G3TTAG construct.

Supplementary Material

Refer to Web version on PubMed Central for supplementary material.

Acknowledgments

We thank Walter Chazin (Vanderbilt University) for generously providing recombinant human replication protein A (R01 GM65484), Thomas Cech (University of Colorado at Boulder) for the flag-tagged telomerase overexpression plasmid, Noah Buncher for technical support on protein purification, Ankur Jain for his help with the telomerase pull-down assay, and Ramreddy Tippana for helpful discussions.

FUNDING

Support for this work was provided by NIH Director's New Innovator Award (343 NIH 1 DP2 GM105453 A) and American Cancer Society (Research Scholar Grant; RSG-12-066-01-DMC) for S. M., Linda Su-Nan Chang Sah Doctoral Fellowship for H. H., NIH grant RO1 ES015632 for P.S., and NIH grant ES0515052 and the David Scaife Foundation for P.L.O.

REFERENCE

Ambrus A, Chen D, Dai J, Bialis T, Jones RA, Yang D. Human telomeric sequence forms a hybrid-type intramolecular G-quadruplex structure with mixed parallel/antiparallel strands in potassium solution. Nucleic Acids Res. 2006; 34:2723–2735. [PubMed: 16714449]

Arata H, Dupont A, Mine-Hattab J, Disseau L, Renodon-Corniere A, Takahashi M, Viovy JL, Cappello G. Direct observation of twisting steps during Rad51 polymerization on DNA. Proc Natl Acad Sci U S A. 2009; 106:19239–19244. [PubMed: 19884492]

Arunkumar AI, Klimovich V, Jiang X, Ott RD, Mizoue L, Fanning E, Chazin WJ. Insights into hRPA32 C-terminal domain--mediated assembly of the simian virus 40 replisome. Nat Struct Mol Biol. 2005; 12:332–339. [PubMed: 15793585]

Bauer L, Tluckova K, Tohova P, Viglasky V. G-quadruplex motifs arranged in tandem occurring in telomeric repeats and the insulin-linked polymorphic region. Biochemistry. 2011; 50:7484–7492. [PubMed: 21819151]

Berman AJ, Akiyama BM, Stone MD, Cech TR. The RNA accordion model for template positioning by telomerase RNA during telomeric DNA synthesis. Nat Struct Mol Biol. 2011; 18:1371–1375. [PubMed: 22101935]

Biffi G, Tannahill D, McCafferty J, Balasubramanian S. Quantitative visualization of DNA G-quadruplex structures in human cells. Nat Chem. 2013; 5:182–186. [PubMed: 23422559]

Bryan TM, Englezou A, Dalla-Pozza L, Dunham MA, Reddel RR. Evidence for an alternative mechanism for maintaining telomere length in human tumors and tumor-derived cell lines. Nat Med. 1997; 3:1271–1274. [PubMed: 9359704]

Bryan TM, Englezou A, Gupta J, Bacchetti S, Reddel RR. Telomere elongation in immortal human cells without detectable telomerase activity. EMBO J. 1995; 14:4240–4248. [PubMed: 7556065]

Burger AM, Dai F, Schultes CM, Reszka AP, Moore MJ, Double JA, Neidle S. The G-quadruplex-interactive molecule BRACO-19 inhibits tumor growth, consistent with telomere targeting and interference with telomerase function. Cancer Res. 2005; 65:1489–1496. [PubMed: 15735037]

Bussen W, Raynard S, Busygina V, Singh AK, Sung P. Holliday junction processing activity of the BLM-Topo IIIalpha-BLAP75 complex. J Biol Chem. 2007; 282:31484–31492. [PubMed: 17728255]

Cesare AJ, Reddel RR. Telomere uncapping and alternative lengthening of telomeres. Mech Ageing Dev. 2008; 129:99–108. [PubMed: 18215414]

Cesare AJ, Reddel RR. Alternative lengthening of telomeres: models, mechanisms and implications. Nat Rev Genet. 2010; 11:319–330. [PubMed: 20351727]

Chen Z, Yang H, Pavletich NP. Mechanism of homologous recombination from the RecA-ssDNA/dsDNA structures. Nature. 2008; 453:489–484. [PubMed: 18497818]

Colgin LM, Baran K, Baumann P, Cech TR, Reddel RR. Human POT1 facilitates telomere elongation by telomerase. Curr Biol. 2003; 13:942–946. [PubMed: 12781132]

Cristofari G, Lingner J. Telomere length homeostasis requires that telomerase levels are limiting. EMBO J. 2006; 25:565–574. [PubMed: 16424902]

d'Adda di Fagagna F, Teo SH, Jackson SP. Functional links between telomeres and proteins of the DNA-damage response. Genes Dev. 2004; 18:1781–1799. [PubMed: 15289453]

de Lange T. How telomeres solve the end-protection problem. Science. 2009; 326:948–952. [PubMed: 19965504]

Denchi EL, de Lange T. Protection of telomeres through independent control of ATM and ATR by TRF2 and POT1. Nature. 2007; 448:1068–1071. [PubMed: 17687332]

Dunham MA, Neumann AA, Fasching CL, Reddel RR. Telomere maintenance by recombination in human cells. Nat Genet. 2000; 26:447–450. [PubMed: 11101843]

Gomez D, O'Donohue MF, Wenner T, Douarre C, Macadre J, Koebel P, Giraud-Panis MJ, Kaplan H, Kolkes A, Shin-ya K, Riou JF. The G-quadruplex ligand telomestatin inhibits POT1 binding to telomeric sequences in vitro and induces GFP-POT1 dissociation from telomeres in human cells. Cancer Res. 2006a; 66:6908–6912. [PubMed: 16849533]

Gomez D, Wenner T, Brassart B, Douarre C, O'Donohue MF, El Khoury V, Shin-Ya K, Morjani H, Trentesaux C, Riou JF. Telomestatin-induced telomere uncapping is modulated by POT1 through G-overhang extension in HT1080 human tumor cells. J Biol Chem. 2006b; 281:38721–38729. [PubMed: 17050546]

Greider CW, Blackburn EH. The telomere terminal transferase of Tetrahymena is a ribonucleoprotein enzyme with two kinds of primer specificity. Cell. 1987; 51:887–898. [PubMed: 3319189]

Griffith JD, Comeau L, Rosenfield S, Stansel RM, Bianchi A, Moss H, de Lange T. Mammalian telomeres end in a large duplex loop. Cell. 1999; 97:503–514. [PubMed: 10338214]

Hardin CC, Henderson E, Watson T, Prosser JK. Monovalent cation induced structural transitions in telomeric DNAs: G-DNA folding intermediates. Biochemistry. 1991; 30:4460–4472. [PubMed: 2021636]

Hardin CC, Watson T, Corregan M, Bailey C. Cation-dependent transition between the quadruplex and Watson-Crick hairpin forms of d(CGCG3GCG). Biochemistry. 1992; 31:833–841. [PubMed: 1731941]

Harley CB, Futcher AB, Greider CW. Telomeres shorten during ageing of human fibroblasts. Nature. 1990; 345:458–460. [PubMed: 2342578]

He F, Tang Y, Wang S, Li Y, Zhu D. Fluorescent amplifying recognition for DNA G-quadruplex folding with a cationic conjugated polymer: a platform for homogeneous potassium detection. J Am Chem Soc. 2005; 127:12343–12346. [PubMed: 16131213]

Henson JD, Cao Y, Huschtscha LI, Chang AC, Au AY, Pickett HA, Reddel RR. DNA C-circles are specific and quantifiable markers of alternative-lengthening-of-telomeres activity. Nat Biotechnol. 2009; 27:1181–1185. [PubMed: 19935656]

Henson JD, Neumann AA, Yeager TR, Reddel RR. Alternative lengthening of telomeres in mammalian cells. Oncogene. 2002; 21:598–610. [PubMed: 11850785]

Hilario J, Amitani I, Baskin RJ, Kowalczykowski SC. Direct imaging of human Rad51 nucleoprotein dynamics on individual DNA molecules. Proc Natl Acad Sci U S A. 2009; 106:361–368. [PubMed: 19122145]

Hockemeyer D, Daniels JP, Takai H, de Lange T. Recent expansion of the telomeric complex in rodents: Two distinct POT1 proteins protect mouse telomeres. Cell. 2006; 126:63–77. [PubMed: 16839877]

Hockemeyer D, Sfeir AJ, Shay JW, Wright WE, de Lange T. POT1 protects telomeres from a transient DNA damage response and determines how human chromosomes end. EMBO J. 2005; 24:2667–2678. [PubMed: 15973431]

Hwang H, Buncher N, Opresko PL, Myong S. POT1-TPP1 Regulates Telomeric Overhang Structural Dynamics. Structure. 2012

Jain A, Liu R, Ramani B, Arauz E, Ishitsuka Y, Ragunathan K, Park J, Chen J, Xiang YK, Ha T. Probing cellular protein complexes using single-molecule pull-down. Nature. 2011; 473:484–488. [PubMed: 21614075]

Karlseder J, Broccoli D, Dai Y, Hardy S, de Lange T. p53- and ATM-dependent apoptosis induced by telomeres lacking TRF2. Science. 1999; 283:1321–1325. [PubMed: 10037601]

Kim NW, Piatyszek MA, Prowse KR, Harley CB, West MD, Ho PL, Coviello GM, Wright WE, Weinrich SL, Shay JW. Specific association of human telomerase activity with immortal cells and cancer. Science. 1994; 266:2011–2015. [PubMed: 7605428]

Lane AN, Chaires JB, Gray RD, Trent JO. Stability and kinetics of G-quadruplex structures. Nucleic Acids Res. 2008; 36:5482–5515. [PubMed: 18718931]

Latrick CM, Cech TR. POT1-TPP1 enhances telomerase processivity by slowing primer dissociation and aiding translocation. EMBO J. 2010; 29:924–933. [PubMed: 20094033]

Lei M, Podell ER, Cech TR. Structure of human POT1 bound to telomeric single-stranded DNA provides a model for chromosome end-protection. Nat Struct Mol Biol. 2004; 11:1223–1229. [PubMed: 15558049]

Lei M, Zaug AJ, Podell ER, Cech TR. Switching human telomerase on and off with hPOT1 protein in vitro. J Biol Chem. 2005; 280:20449–20456. [PubMed: 15792951]

Lingner J, Cooper JP, Cech TR. Telomerase and DNA end replication: no longer a lagging strand problem? Science. 1995; 269:1533–1534. [PubMed: 7545310]

Liu JQ, Chen CY, Xue Y, Hao YH, Tan Z. G-quadruplex hinders translocation of BLM helicase on DNA: a real-time fluorescence spectroscopic unwinding study and comparison with duplex substrates. J Am Chem Soc. 2010; 132:10521–10527. [PubMed: 20614884]

Lundblad V, Blackburn EH. An alternative pathway for yeast telomere maintenance rescues est1- senescence. Cell. 1993; 73:347–360. [PubMed: 8477448]

Makarov VL, Hirose Y, Langmore JP. Long G tails at both ends of human chromosomes suggest a C strand degradation mechanism for telomere shortening. Cell. 1997; 88:657–666. [PubMed: 9054505]

McElligott R, Wellinger RJ. The terminal DNA structure of mammalian chromosomes. EMBO J. 1997; 16:3705–3714. [PubMed: 9218811]

Mendez-Bermudez A, Hidalgo-Bravo A, Cotton VE, Gravani A, Jeyapalan JN, Royle NJ. The roles of WRN and BLM RecQ helicases in the Alternative Lengthening of Telomeres. Nucleic Acids Res. 2012; 40:10809–10820. [PubMed: 22989712]

Mohaghegh P, Karow JK, Brosh RM Jr. Bohr VA, Hickson ID. The Bloom's and Werner's syndrome proteins are DNA structure-specific helicases. Nucleic Acids Res. 2001; 29:2843–2849. [PubMed: 11433031]

Murphy MC, Rasnik I, Cheng W, Lohman TM, Ha T. Probing single-stranded DNA conformational flexibility using fluorescence spectroscopy. Biophys J. 2004; 86:2530–2537. [PubMed: 15041689]

Oganesian L, Karlseder J. Mammalian 5′ C-rich telomeric overhangs are a mark of recombination-dependent telomere maintenance. Mol Cell. 2011; 42:224–236. [PubMed: 21504833]

Opresko PL, Sowd G, Wang H. The Werner syndrome helicase/exonuclease processes mobile D-loops through branch migration and degradation. PLoS One. 2009; 4:e4825. [PubMed: 19283071]

Paeschke K, Bochman ML, Garcia PD, Cejka P, Friedman KL, Kowalczykowski SC, Zakian VA. Pif1 family helicases suppress genome instability at G-quadruplex motifs. Nature. 2013; 497:458–462. [PubMed: 23657261]

Paeschke K, Capra JA, Zakian VA. DNA replication through G-quadruplex motifs is promoted by the Saccharomyces cerevisiae Pif1 DNA helicase. Cell. 2011; 145:678–691. [PubMed: 21620135]

Palm W, de Lange T. How shelterin protects mammalian telomeres. Annu Rev Genet. 2008; 42:301–334. [PubMed: 18680434]

Palm W, Hockemeyer D, Kibe T, de Lange T. Functional dissection of human and mouse POT1 proteins. Mol Cell Biol. 2009; 29:471–482. [PubMed: 18955498]

Petraccone L, Spink C, Trent JO, Garbett NC, Mekmaysy CS, Giancola C, Chaires JB. Structure and stability of higher-order human telomeric quadruplexes. J Am Chem Soc. 2011; 133:20951–20961. [PubMed: 22082001]

Phatak P, Cookson JC, Dai F, Smith V, Gartenhaus RB, Stevens MF, Burger AM. Telomere uncapping by the G-quadruplex ligand RHPS4 inhibits clonogenic tumour cell growth in vitro and in vivo consistent with a cancer stem cell targeting mechanism. Br J Cancer. 2007; 96:1223–1233. [PubMed: 17406367]

Salazar M, Thompson BD, Kerwin SM, Hurley LH. Thermally induced DNA.RNA hybrid to G-quadruplex transitions: possible implications for telomere synthesis by telomerase. Biochemistry. 1996; 35:16110–16115. [PubMed: 8973182]

Sfeir A, Kosiyatrakul ST, Hockemeyer D, MacRae SL, Karlseder J, Schildkraut CL, de Lange T. Mammalian telomeres resemble fragile sites and require TRF1 for efficient replication. Cell. 2009; 138:90–103. [PubMed: 19596237]

Shakirov EV, Surovtseva YV, Osbun N, Shippen DE. The Arabidopsis Pot1 and Pot2 proteins function in telomere length homeostasis and chromosome end protection. Mol Cell Biol. 2005; 25:7725–7733. [PubMed: 16107718]

Shampay J, Szostak JW, Blackburn EH. DNA sequences of telomeres maintained in yeast. Nature. 1984; 310:154–157. [PubMed: 6330571]

Shay JW, Bacchetti S. A survey of telomerase activity in human cancer. Eur J Cancer. 1997; 33:787–791. [PubMed: 9282118]

Shay JW, Wright WE. Telomerase: a target for cancer therapeutics. Cancer Cell. 2002; 2:257–265. [PubMed: 12398889]

Shin DS, Pellegrini L, Daniels DS, Yelent B, Craig L, Bates D, Yu DS, Shivji MK, Hitomi C, Arvai AS, et al. Full-length archaeal Rad51 structure and mutants: mechanisms for RAD51 assembly and control by BRCA2. EMBO J. 2003; 22:4566–4576. [PubMed: 12941707]

Sigurdsson S, Trujillo K, Song B, Stratton S, Sung P. Basis for avid homologous DNA strand exchange by human Rad51 and RPA. J Biol Chem. 2001; 276:8798–8806. [PubMed: 11124265]

Smogorzewska A, de Lange T. Different telomere damage signaling pathways in human and mouse cells. EMBO J. 2002; 21:4338–4348. [PubMed: 12169636]

Stavropoulos DJ, Bradshaw PS, Li X, Pasic I, Truong K, Ikura M, Ungrin M, Meyn MS. The Bloom syndrome helicase BLM interacts with TRF2 in ALT cells and promotes telomeric DNA synthesis. Hum Mol Genet. 2002; 11:3135–3144. [PubMed: 12444098]

Tahara H, Shin-Ya K, Seimiya H, Yamada H, Tsuruo T, Ide T. G-Quadruplex stabilization by telomestatin induces TRF2 protein dissociation from telomeres and anaphase bridge formation accompanied by loss of the 3′ telomeric overhang in cancer cells. Oncogene. 2006; 25:1955–1966. [PubMed: 16302000]

Takai KK, Kibe T, Donigian JR, Frescas D, de Lange T. Telomere protection by TPP1/POT1 requires tethering to TIN2. Mol Cell. 2011; 44:647–659. [PubMed: 22099311]

Tang J, Kan ZY, Yao Y, Wang Q, Hao YH, Tan Z. G-quadruplex preferentially forms at the very 3′ end of vertebrate telomeric DNA. Nucleic Acids Res. 2008; 36:1200–1208. [PubMed: 18158301]

Tarkanyi I, Aradi J. Pharmacological intervention strategies for affecting telomerase activity: future prospects to treat cancer and degenerative disease. Biochimie. 2008; 90:156–172. [PubMed: 17945408]

Tarsounas M, Munoz P, Claas A, Smiraldo PG, Pittman DL, Blasco MA, West SC. Telomere maintenance requires the RAD51D recombination/repair protein. Cell. 2004; 117:337–347. [PubMed: 15109494]

van Mameren J, Modesti M, Kanaar R, Wyman C, Peterman EJ, Wuite GJ. Counting RAD51 proteins disassembling from nucleoprotein filaments under tension. Nature. 2009; 457:745–748. [PubMed: 19060884]

Vannier JB, Pavicic-Kaltenbrunner V, Petalcorin MI, Ding H, Boulton SJ. RTEL1 dismantles T loops and counteracts telomeric G4-DNA to maintain telomere integrity. Cell. 2012; 149:795–806. [PubMed: 22579284]

Varley H, Pickett HA, Foxon JL, Reddel RR, Royle NJ. Molecular characterization of inter-telomere and intra-telomere mutations in human ALT cells. Nat Genet. 2002; 30:301–305. [PubMed: 11919561]

Vorlickova M, Chladkova J, Kejnovska I, Fialova M, Kypr J. Guanine tetraplex topology of human telomere DNA is governed by the number of (TTAGGG) repeats. Nucleic Acids Res. 2005; 33:5851–5860. [PubMed: 16221978]

Wang H, Nora GJ, Ghodke H, Opresko P. Single Molecule Studies of Physiologically Relevant Telomeric Tails Reveals Pot1 Mechanism for Promoting G-Quadruplex Unfolding. J Biol Chem. 2010

Wang Q, Liu JQ, Chen Z, Zheng KW, Chen CY, Hao YH, Tan Z. G-quadruplex formation at the 3′ end of telomere DNA inhibits its extension by telomerase, polymerase and unwinding by helicase. Nucleic Acids Res. 2011; 39:6229–6237. [PubMed: 21441540]

Watson JD. Origin of concatemeric T7 DNA. Nat New Biol. 1972; 239:197–201. [PubMed: 4507727]

Weinrich SL, Pruzan R, Ma L, Ouellette M, Tesmer VM, Holt SE, Bodnar AG, Lichtsteiner S, Kim NW, Trager JB, et al. Reconstitution of human telomerase with the template RNA component hTR and the catalytic protein subunit hTRT. Nat Genet. 1997; 17:498–502. [PubMed: 9398860]

Wong A, Wu G. Selective binding of monovalent cations to the stacking G-quartet structure formed by guanosine 5′-monophosphate: a solid-state NMR study. J Am Chem Soc. 2003; 125:13895–13905. [PubMed: 14599230]

Wright WE, Tesmer VM, Huffman KE, Levene SD, Shay JW. Normal human chromosomes have long G-rich telomeric overhangs at one end. Genes Dev. 1997; 11:2801–2809. [PubMed: 9353250]

Wu L, Multani AS, He H, Cosme-Blanco W, Deng Y, Deng JM, Bachilo O, Pathak S, Tahara H, Bailey SM, et al. Pot1 deficiency initiates DNA damage checkpoint activation and aberrant homologous recombination at telomeres. Cell. 2006; 126:49–62. [PubMed: 16839876]

Ye JZ, Hockemeyer D, Krutchinsky AN, Loayza D, Hooper SM, Chait BT, de Lange T. POT1-interacting protein PIP1: a telomere length regulator that recruits POT1 to the TIN2/TRF1 complex. Genes Dev. 2004; 18:1649–1654. [PubMed: 15231715]

Yu HQ, Miyoshi D, Sugimoto N. Characterization of structure and stability of long telomeric DNA G-quadruplexes. J Am Chem Soc. 2006; 128:15461–15468. [PubMed: 17132013]

Zahler AM, Williamson JR, Cech TR, Prescott DM. Inhibition of telomerase by G-quartet DNA structures. Nature. 1991; 350:718–720. [PubMed: 2023635]

Zaug AJ, Podell ER, Cech TR. Human POT1 disrupts telomeric G-quadruplexes allowing telomerase extension in vitro. Proc Natl Acad Sci U S A. 2005; 102:10864–10869. [PubMed: 16043710]

Zaug AJ, Podell ER, Nandakumar J, Cech TR. Functional interaction between telomere protein TPP1 and telomerase. Genes Dev. 2010; 24:613–622. [PubMed: 20231318]

Zhang Y, Chen LY, Han X, Xie W, Kim H, Yang D, Liu D, Songyang Z. Phosphorylation of TPP1 regulates cell cycle-dependent telomerase recruitment. Proc Natl Acad Sci U S A. 2013; 110:5457–5462. [PubMed: 23509301]

HIGHLIGHTS

- Telomeric overhang exhibits dynamic behavior when greater than four TTAGGG repeats
- Four and eight repeats yield low accessibility to WRN, BLM, Rad51 and telomerase
- Five to seven repeats yield increased accessibility to loading of the same proteins
- POT1 bind all repeat lengths proficiently, suggesting an active disruption of GQ

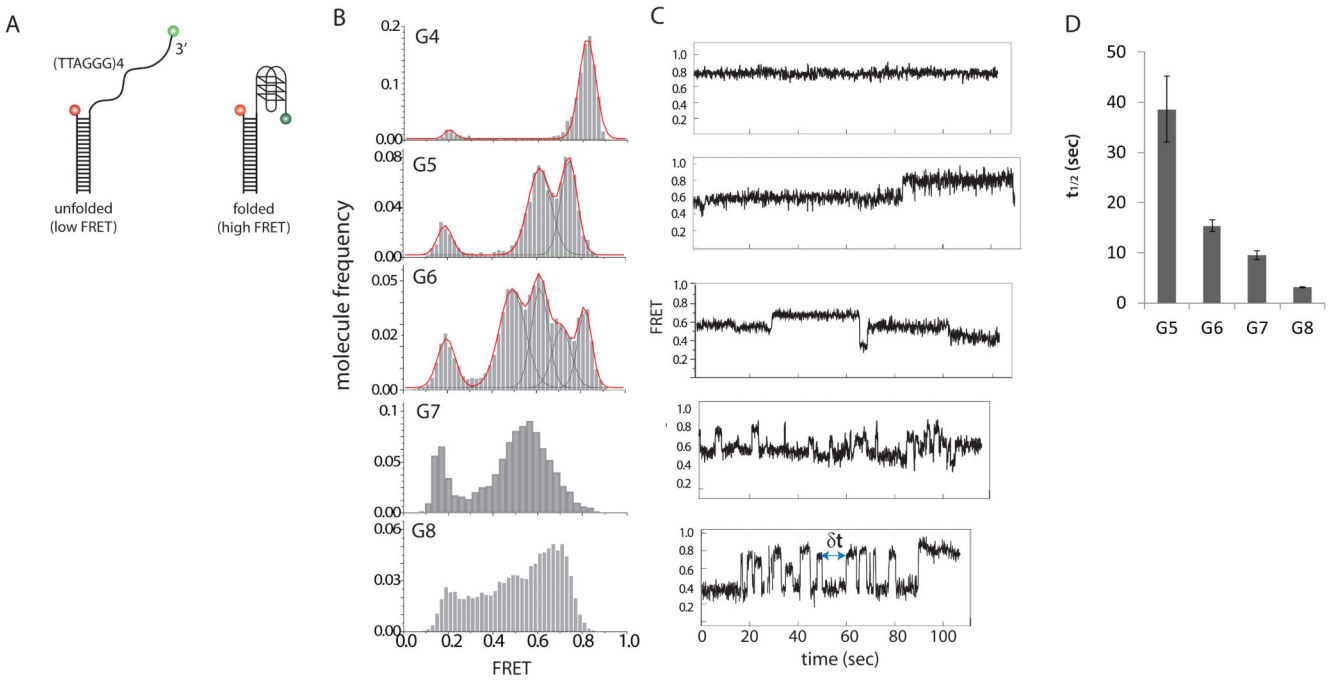

Figure 1.

(A) Schematic of DNA used for single molecule FRET. Two dyes, Cy3 and Cy5 are attached to both sides of 4 repeats of TTAGGG. High FRET and low FRET correspond to folding and unfolding of G-quadruplex (GQ), respectively. (B) Single molecule frequency histograms of DNA with 4, 5, 6, 7, and 8 repeats of TTAGGG. The red outline is the summation of 1, 2, and 4 Gaussian fits for G4, G5, and G6 respectively. (C) Representative single molecule trace for G4-G8. (D) Plot of half time, $t_{1/2}$ obtained from fitting dwell times to exponential decay. (dwell times are denoted by blue arrow in single molecule trace)

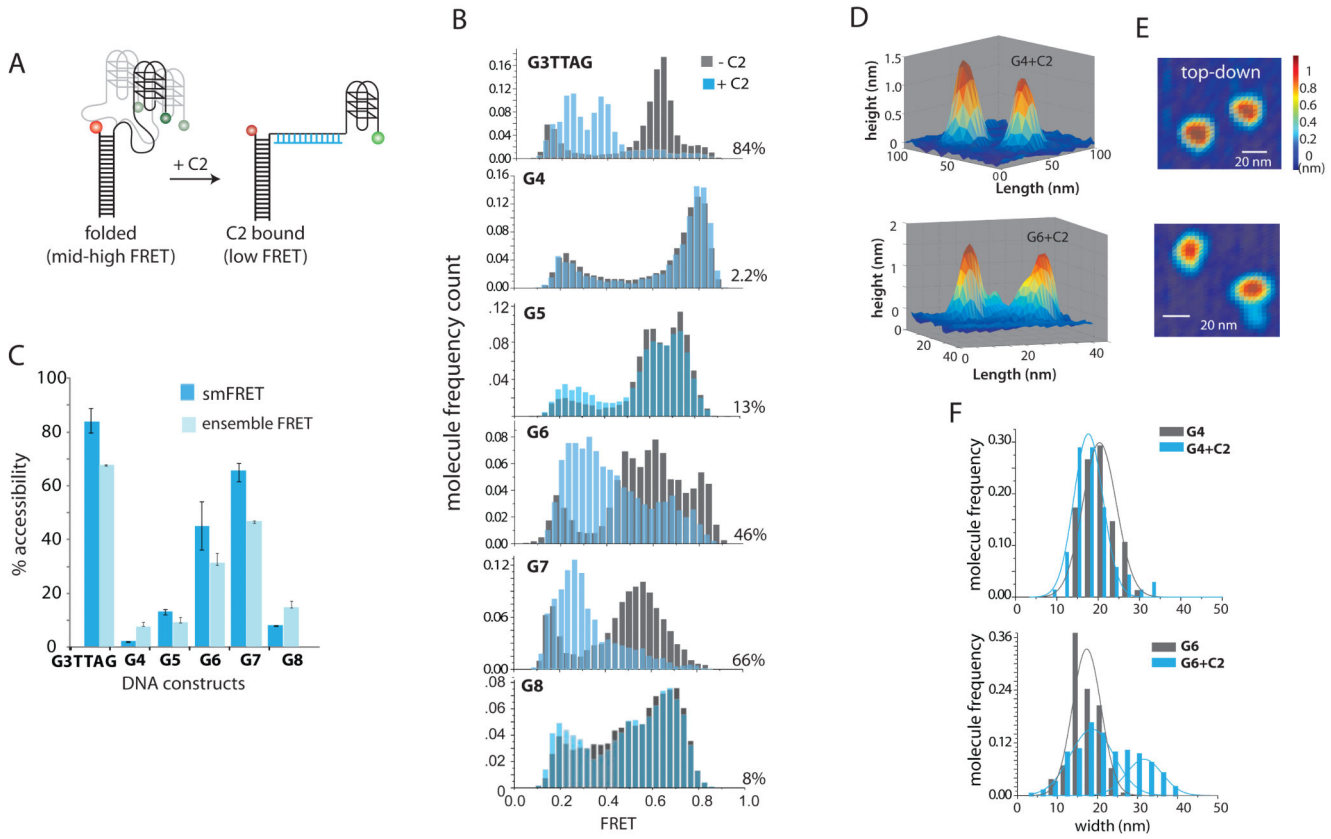

Figure 2.

(A) Schematic of complementary 12-mer, C2, binding to single stranded portions of the telomeric overhang repeats. (B) Frequency count histograms before and after binding of C2 to G3TTAG and G4-G8. (C) Percent accessibility calculated for single molecule and ensemble FRET. (D) Example contour plots (side view) and (E) top-down view of two G4 molecules and two G6 molecules incubated with C2, imaged with atomic force microscopy (AFM). (F) Width distribution histograms of molecules for G4 and G6 before and after the addition of C2 collected by AFM imaging.

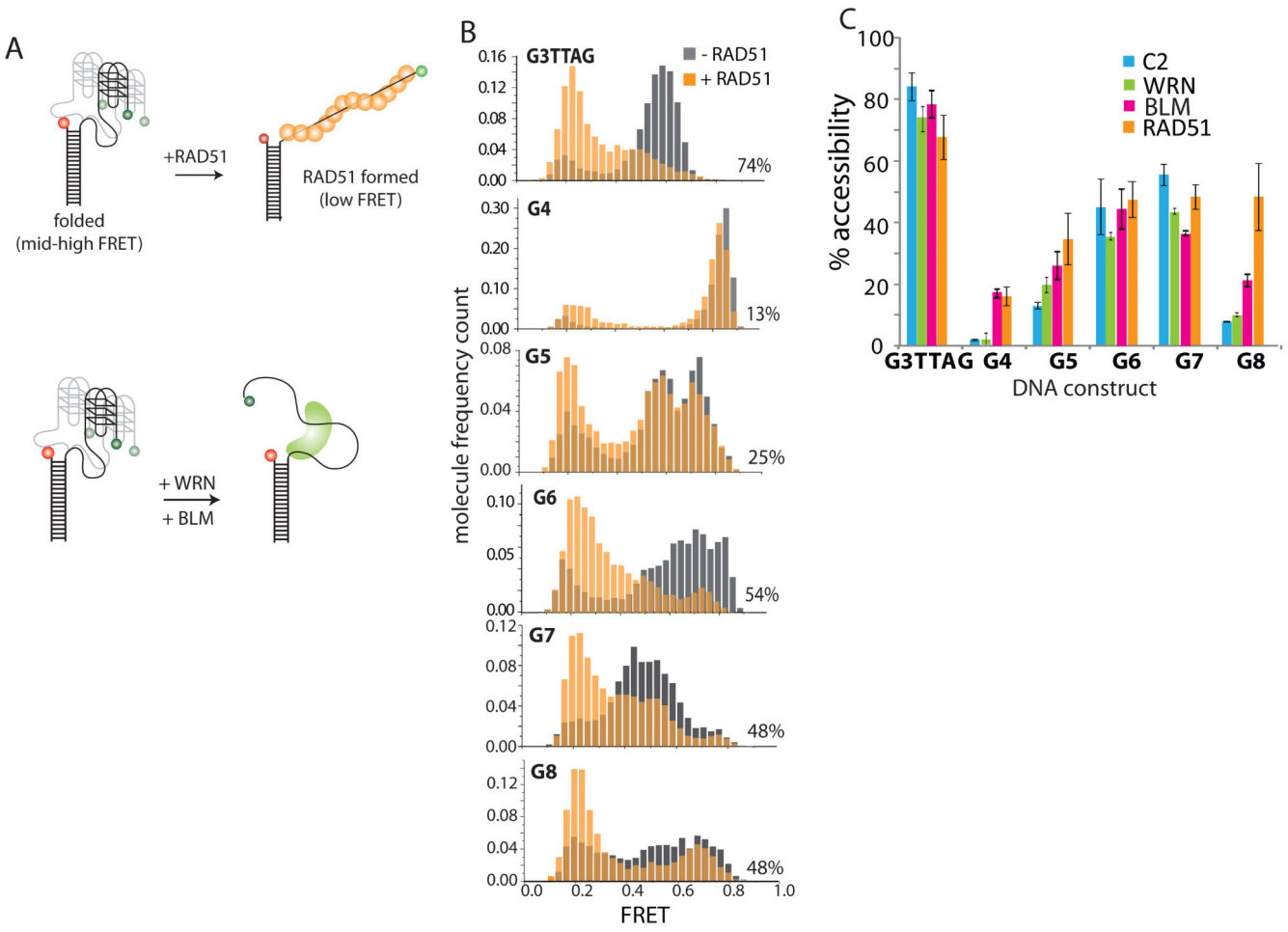

Figure 3.

(A) Schematic of RAD51 and RecQ helicases (WRN and BLM) to DNA. (B) Frequency count histogram before and after addition of RAD51 on G3TTAG and G4-G8. (C) Summary plot comparing percent accessibility between RAD51, WRN, BLM and C2 for increasing repeat numbers of the telomere overhang

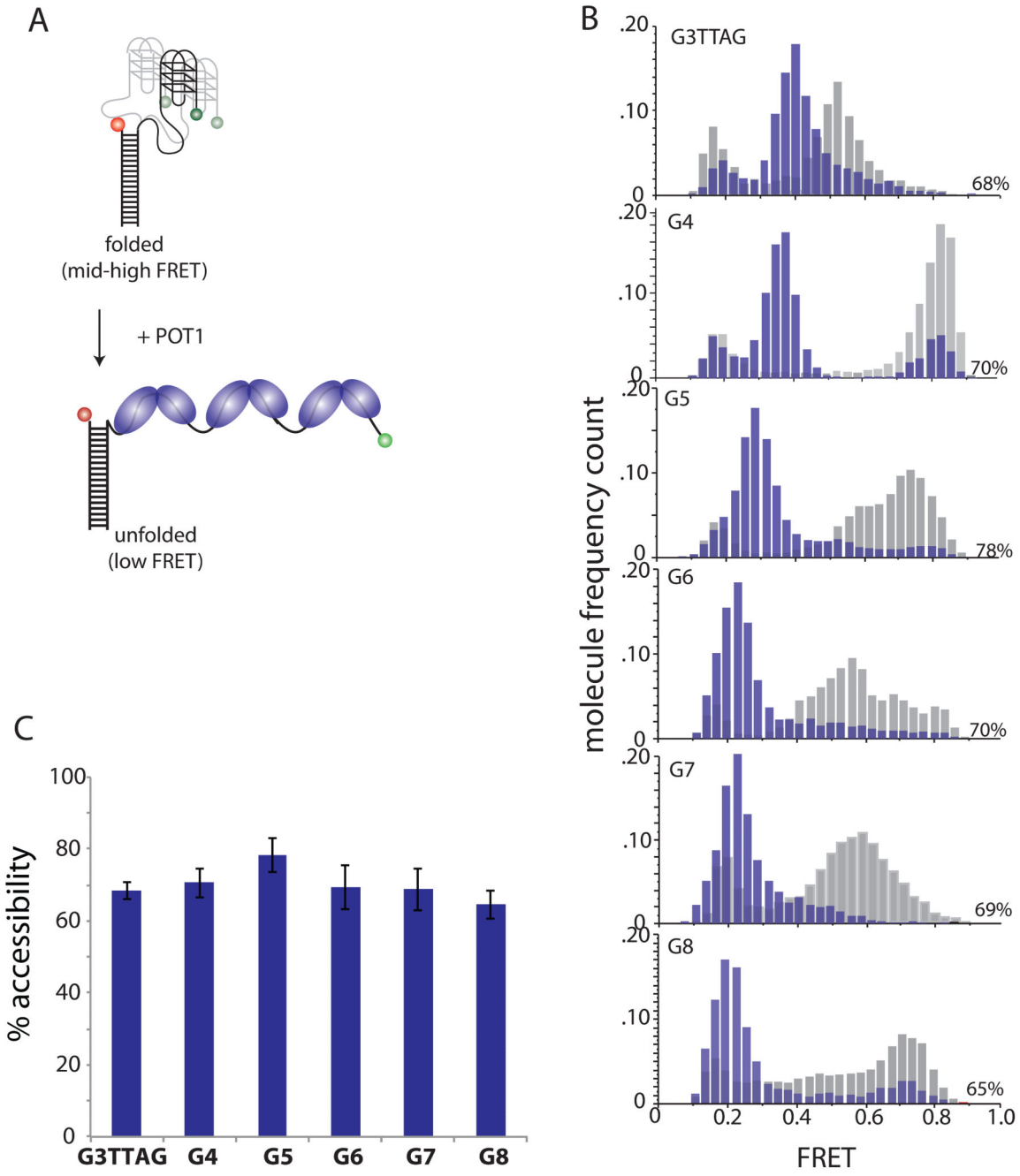

Figure 4.

(A) Schematic of POT1 unfolding the telomeric DNA. (B) Molecule frequency count histograms before and after addition of POT1 for G3TTAG and G4-G8 DNA. (C) Plot of percent accessibility for POT1 binding to increasing number of telomere overhang.

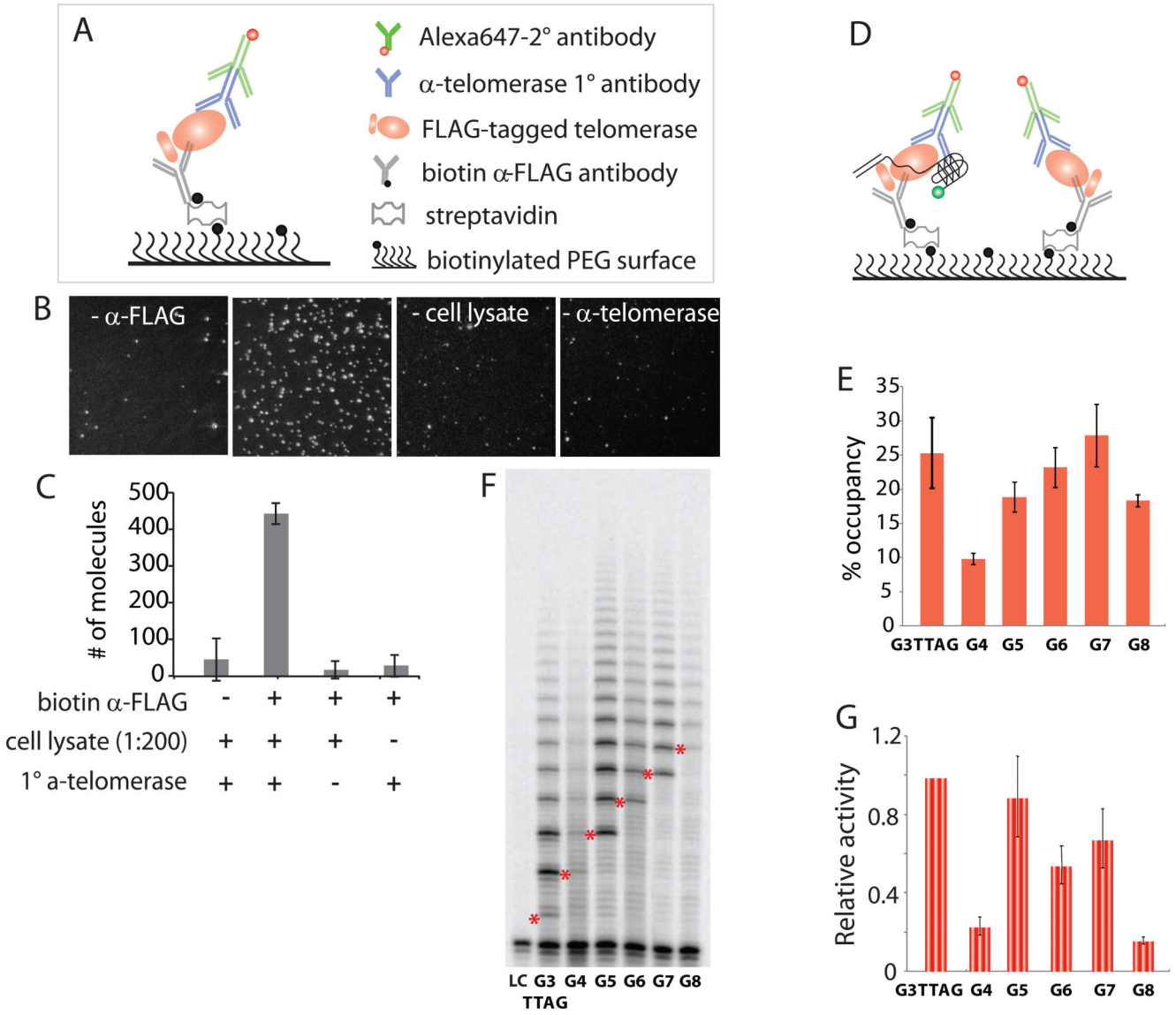

Figure 5.

(A) Schematic of single molecule pull-down of overexpressed telomerase (flag-tagged) from HEK293T cells. (B) Images and (C) quantification of molecules pulled down demonstrating the specificity of telomerase capture. (D) Schematic of colocalization of telomerase (Alex 647 labeled antibody) and Cy3-labeled telomeric DNA. (E) Percent occupancy of DNA to telomerase calculated by the percent of colocalization. (F) Gel image from primer extension assay with various repeat length constructs. (G) Quantification of extension activity by using Image J and Image Quant.